AUTHOR and OTHER-AUTHOR

[Left hand page running head is author's name in Times New Roman 8 point bold capitals, centred. For more than two authors, write **AUTHOR et al.**]

CONFERENCE PRE-PRINT

Design and Testing of Quench Protection System for ITER Magnet Cold Test Bench

WEI TONG (Corresponding Author) Hefei University of Technology Hefei, China Email: tongwei@hfut.edu.cn

HUA LI

Hefei Institutes of Physical Science, Chinese Academy of Sciences Hefei, China

ZHENHAN LI Hefei University of Technology Hefei, China

Abstract

The ITER-MCTB project is a crucial component of the International Thermonuclear Experimental Reactor (ITER) program, playing an important role in advancing sustainable and clean nuclear fusion energy. The quench protection system (QPS) is essential for the safe operation of the tokamak device. The paper focuses on the design and optimization of the QPS to meet the 70 kA/4.1 kV parameter requirements. Specifically, it proposes a permanent magnet bistable actuator to enhance the response performance of the mechanical bypass switch (BPS), designs an electromagnetic repulsion mechanism to improve the switching speed of the vacuum circuit breaker (VCB), optimizes parameters in the auxiliary oscillation zero-crossing loop, and introduces a spiral pulse reactor to improve conversion efficiency and stability. Additionally, a self-disturbing arc contact structure is introduced to enhance the heat dissipation and current-carrying capacity of the pyro-breaker (PB). Finally, 72 breaking tests were conducted at 70 kA, achieving an interruption response time of ≤240 ms. The results demonstrate that the proposed system significantly improves the response speed and reliability of the QPS.

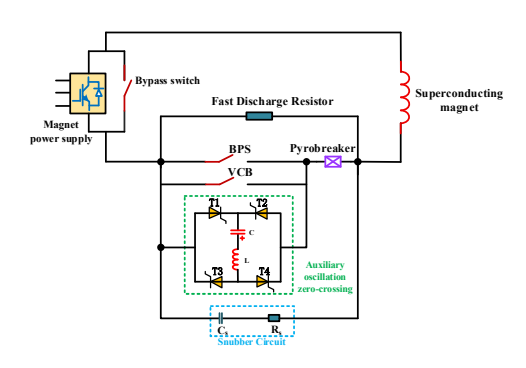
1. INTRODUCTION

Controlled nuclear fusion, as a form of clean energy, is widely regarded as having the potential to reshape the global energy landscape. Unlike traditional fossil fuels and nuclear fission energy, the nuclear fusion process does not produce greenhouse gas emissions or generate long-lived radioactive waste, making it an ideal clean energy source [1,2]. In controlled nuclear fusion technology, superconducting magnets play a critical role by generating strong magnetic fields to confine and stabilize high-temperature, high-density fusion plasma, thereby sustaining the fusion reaction [3-5]. However, superconducting magnets may experience an increase in conductor resistance due to factors such as inter-layer friction, which generates significant Joule heat, causing a sharp rise of temperature in the magnet and leading to irreversible damage to the superconducting state, known as "quenching"[6]. Therefore, the quench protection system (QPS) is crucial for ensuring the safe and reliable operation of the tokamak device [7].

In FIG.1, the mechanical bypass switch (BPS) and vacuum circuit breaker (VCB) form a high-power mechanical switch, while the pre-charged capacitor, pulse reactor, and four sets of thyristor switches constitute an improved H-bridge structure for the conversion circuit. The pyro-breaker (PB) acts as a backup protection switch for the main switch, with fast discharge resistor resistors (FDR) in parallel across the switch, serving as the magnet energy release unit. After the thyristor receives a trigger signal to conduct the conversion circuit, the pre-charged capacitor and reactor form a resonant circuit, generating a pulse current that flows in reverse into the VCB, providing a current zero-crossing point to complete the vacuum switch zero-crossing turn-off. The snubber circuit is used to reduce the rate of change of the reverse recovery voltage across the VCB at the moment of current zero-crossing, and it also helps reduce the reverse voltage during the conversion process caused by parasitic parameters in the circuit. In FIG.2, the control logic of the QPS and the expected waveforms of the current transfer process in each branch [8-10]. The QPS has developed a relatively complete technical solution in terms of structure and operating principle. However, when facing the higher response speed and reliability requirements of the MCTB device, the existing design still shows some inadequacies.

This paper systematically designs and optimizes the key components of the QPS based on the parameter requirements of ITER-MCTB. First, a permanent magnet bistable actuator is designed to enhance the switching speed and operational stability of the BPS. Second, an electromagnetic repulsion mechanism is proposed for the

VCB to effectively improve its response performance. In the auxiliary oscillation zero-crossing loop, the parameters were calculated and optimized, and a spiral pulse reactor was designed to enhance the efficiency and stability of the commutation process. At the same time, a self-disturbing arc contact structure is proposed for the PB to improve its heat dissipation and current-carrying capacity. Finally, after 72 reliability breaking tests, the efficiency and stability of the designed system are fully verified.



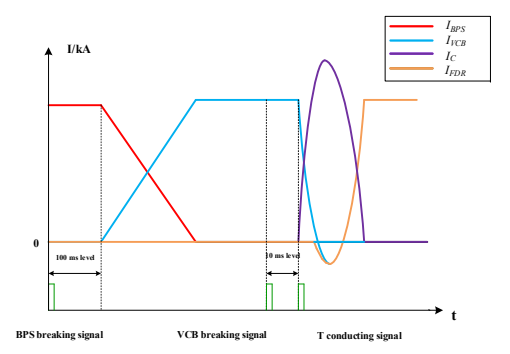


Fig.1. Topology diagram of the QPS.

Fig.2. The control logic of the QPS and expected current waveform.

2. OVERVIEW OF QPS MECHANISM

The current transfer during the working process of the QPS is shown in FIG.3 [11-12]. In FIG.3(a), during normal operation, both the BPS and VCB are closed, the system load current primarily flows through the BPS branch. In FIG.3(b), When a quench is detected, the BPS opens and generates an arc. Under the arc voltage, the current in the BPS branch rapidly decreases and is fully transferred to the VCB branch. In FIG.3(c), once the BPS has regained sufficient voltage-blocking capability, it begins to interrupt the VCB. At the same time, the thyristors are triggered into conduction. The pre-charged discharge capacitor releases energy through the inductor into the VCB branch, generating an artificial current zero, which forces the VCB current to decrease rapidly until it reaches zero, at which point the VCB is fully disconnected. In FIG.3(d), the current is completely transferred to the FDR, which dissipates the magnet energy in the form of heat, thereby protecting the magnet.

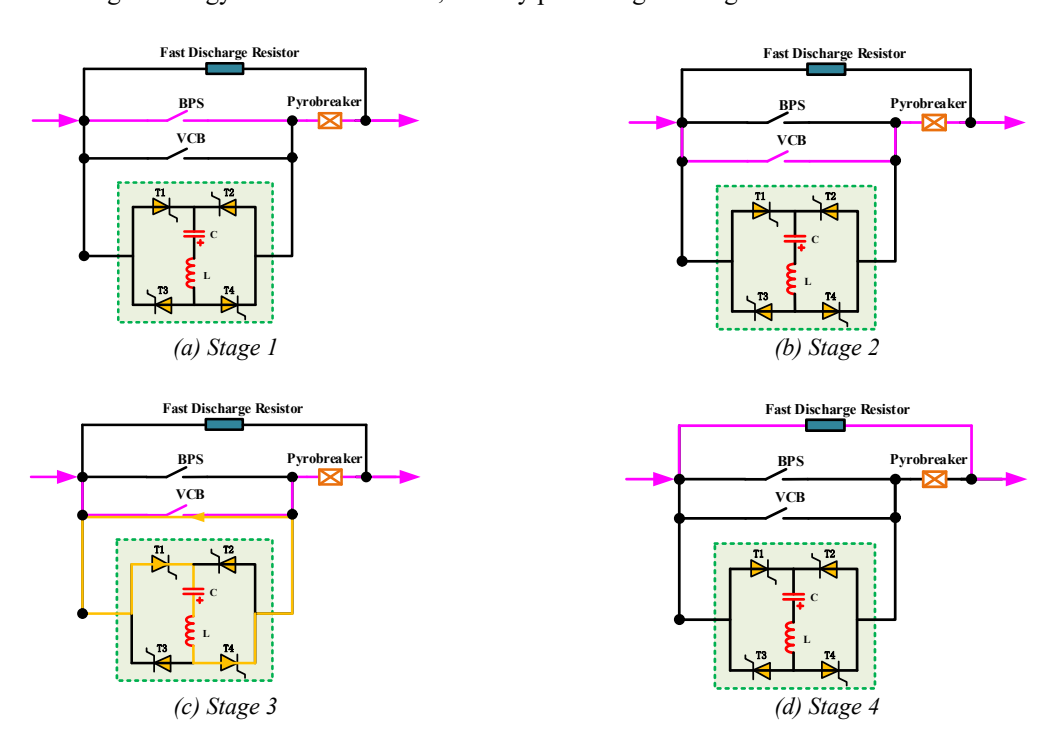


FIG.3. The current transfer diagram when the QPS operates.

DESIGN AND SIMULATION OF QPS

3.1. Design and analysis of key components of BPS

As shown in FIG.4, the BPS is mainly composed of the contact system, permanent magnet bistable actuator, and crank-slider drive mechanism. Through the collaborative action of these components, the BPS meets the high-speed breaking requirements while ensuring compact structure and operational reliability.

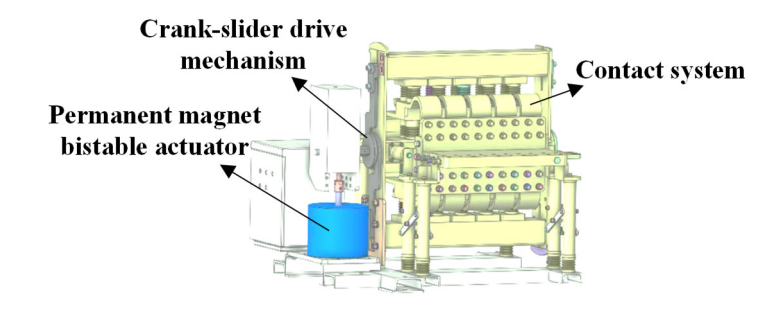


FIG.4. The structural diagram of the BPS.

As shown in FIG.5, the structure of the permanent magnet bistable actuator mainly consists of the moving iron core, open/close coils, push spring, permanent magnet limit rings and drive shaft. The permanent magnet bistable actuator has fewer moving parts, resulting in less mechanical wear, longer mechanical life, and lower maintenance costs.

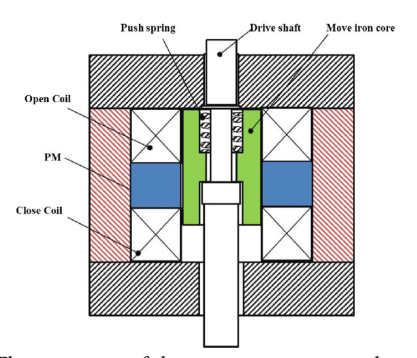


FIG.5. The structure of the permanent magnet bistable actuator.

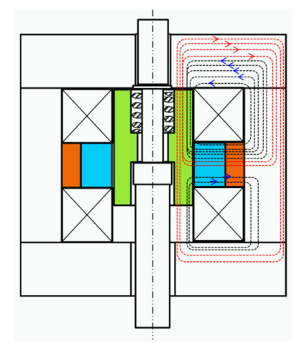


FIG.6. Magnetic flux distribution of the permanent magnet actuator

The closed state is shown in FIG.6, where the black arrow lines represent the magnetic field generated by the permanent magnet, and the red lines represent the opposite magnetic field generated by the excitation of the open coil. Once the trip command from the relay protection is received, the trip coil is excited by a pulse current, rapidly generating a magnetic field opposite to that of the permanent magnet. The coil generates a magnetic field that opposes the magnetic flux lines of the permanent magnet, causing the closing holding force to quickly decrease to zero. A 3D model of the permanent magnet bistable actuator is created using Ansys/Maxwell. The simulation results of opening and closing are shown in FIG.7 and FIG.8.

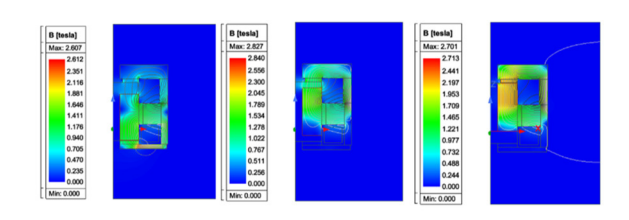


FIG.7. The closing operation of the permanent magnet actuator.

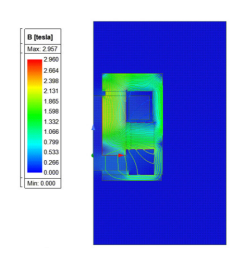


FIG.8. The opening operation of the permanent magnet actuator.

During the opening and closing operations of the mechanism, key components such as the gear, turntable, connecting rods, and beam are subjected to impact loads. These loads may cause fatigue, deformation, or damage to the components, thereby affecting the performance and reliability of the mechanism. By performing computational simulations in Ansys, the stress distribution, deformation, and safety factors of each key component are analyzed, providing reliable data for the design and ensuring the safety and durability of the structure.

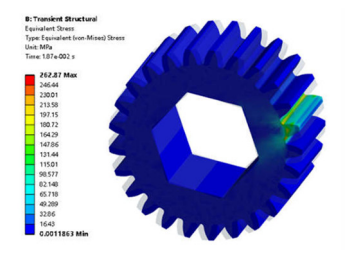


FIG.9. Von Mises stress of the gear.

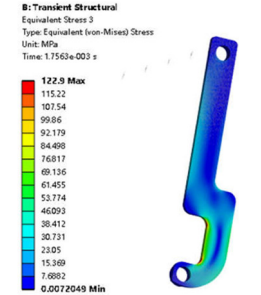


FIG.11. Von mises stress of the connecting rods.

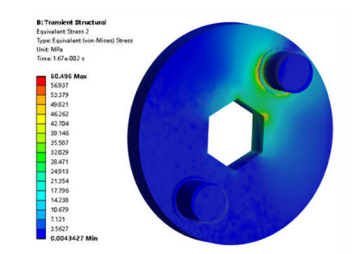


FIG. 10. Von Mises stress of the turntable.

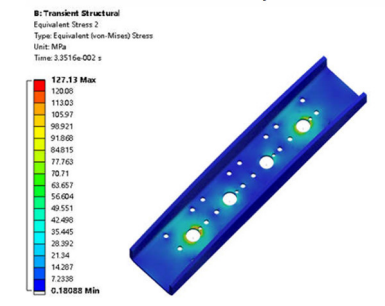


FIG.12. The mises stress of the beam

The stress analysis of the transmission gear and turntable is shown in FIG.9 and FIG.10, respectively. The maximum Mises stress of the gear is 262 MPa, which is less than the yield strength of 830 MPa, indicating that it will not undergo plastic deformation during operation. The maximum Mises stress of the turntable is 60 MPa, which is below the yield strength of 310 MPa, ensuring it has adequate safety margin.

Next, the stress analysis of the connecting rod and beam is carried out, with the results shown in FIG.11 and FIG.12, respectively. The maximum Mises stress of the connecting rod and the beam are 122 MPa and 127 MPa, which is less than the yield strength of 310 MPa. The analysis indicates that the strength of the key components meets the allowable stress requirements, and the safety factor is greater than or equal to 1.3, ensuring their reliability and safety under actual working conditions.

3.2. Design and analysis of key components of VCB

The VCB structure design is shown in FIG.13. It mainly consists of the vacuum arc extinguishing chamber, pulse electromagnetic repulsion mechanism, insulating rod, and control circuit. The VCB adopts a double-break structure to enhance the dielectric recovery strength.

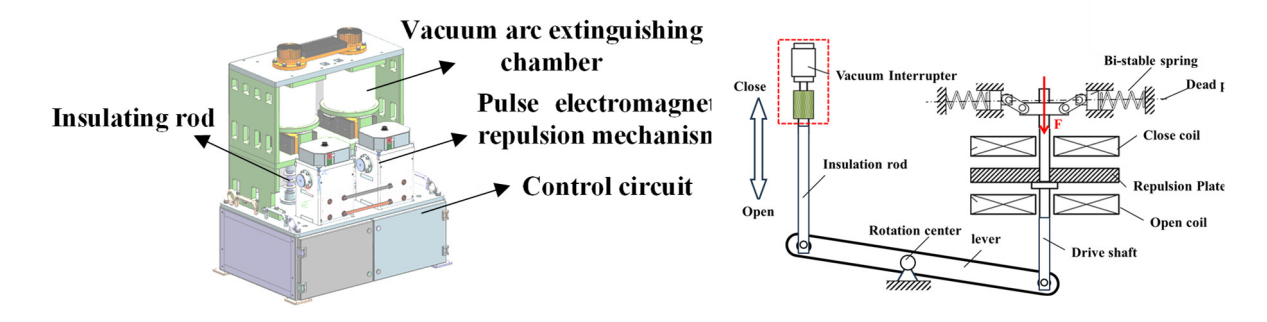


FIG.13. The structure diagram of VCB.

In the design, higher requirements are placed on the drive speed and reliability of the VCB drive unit, and key technical issues such as achieving a break time shorter than the breaking time and ensuring consistent double-

[Left hand page running head is author's name in Times New Roman 8 point bold capitals, centred. For more than two authors, write AUTHOR et al.]

break actions need to be addressed. Traditional drive methods, such as hydraulic, motor, spring, and pneumatic drives, all suffer from issues related to insufficient action speed or control accuracy in vacuum switch applications. The design of the pulse electromagnetic repulsion mechanism offers extremely fast response speed and high control accuracy, enabling effective opening actions within milliseconds of contact separation. This mechanism meets the drive requirements for the motion quality of double-break series vacuum switches.

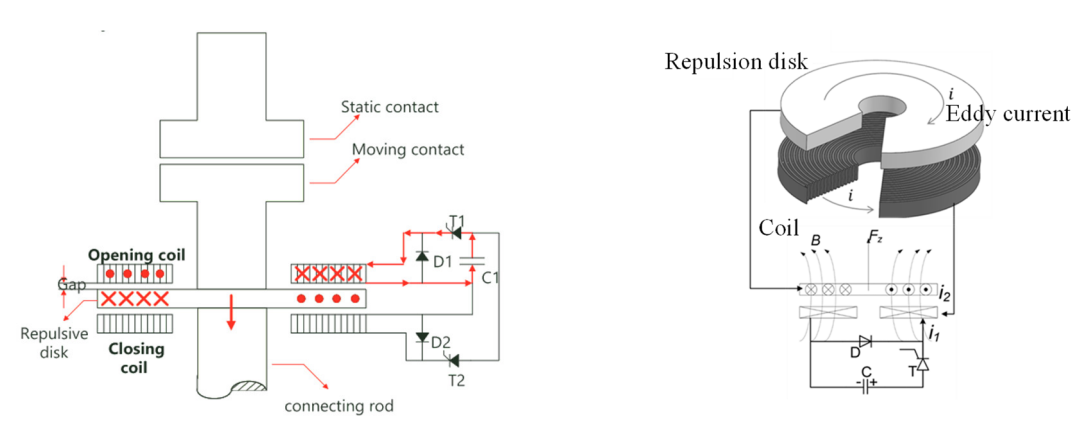


FIG.14. Schematic diagram of electromagnetic repulsion mechanism.

The principle of the electromagnetic repulsion mechanism is shown in FIG.14. When the control of T1 or T2 causes the corresponding opening or closing coil to discharge, the pulse current in the coil generates a rapidly changing magnetic field in the surrounding space. The repulsion plate will produce reverse induced eddy currents under the axial component of the coil's magnetic field and experience a repulsive electromagnetic force under the radial component of the magnetic field. At this point, the repulsion plate will move towards the direction of the other coil, driving the linkage connected to the repulsion plate to operate. Finally, under the push of the linkage, the moving contact and the stationary contact generate the opening and closing actions.

A simulation of the closing operation of the repulsion mechanism has been conducted, and the calculation results are as shown in FIG.15.

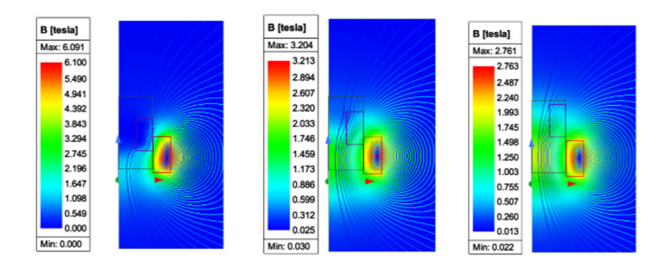


FIG.15. Repulsive mechanism opening simulation.

3.3. Design and analysis of key components of auxiliary oscillation zero-crossing

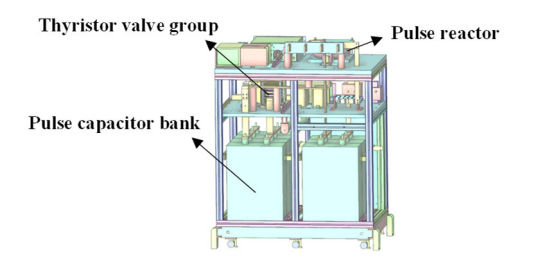
The auxiliary oscillation zero-crossing cabinet structure design is shown in FIG.16. It mainly consists of the pulse capacitor bank, pulse reactor, and thyristor valve group. This circuit utilizes oscillation in the loop to generate a pulse current, which forces the VCB current to decrease, providing an artificial zero-crossing point for the VCB.

Set the maximum rate of rise of the pulse current |di/dt| max| = 200 A/µs. Considering the use of two vacuum arc extinguishing chambers in series in the vacuum circuit breaker, the inductance of the pulse inductance can be calculated by the following equation:

$$L = \frac{U_{co}}{\left| di / dt_{\text{max}} \right|} \tag{1}$$

The capacitance of the storage capacitor can be calculated by equation (1), which is 7.96 mF. To ensure the discharge reliability of the CPC, the capacitance of the capacitor is rounded to 8.0 mF. The pulse inductance is 20 μΗ.

The planar pulse reactor can meet the pulse discharge requirements of the commutation circuit, its inherent leakage magnetic phenomenon may have adverse effects on surrounding equipment. Design a ring-shaped spiral pulse reactor, with its structure shown in the FIG.17.



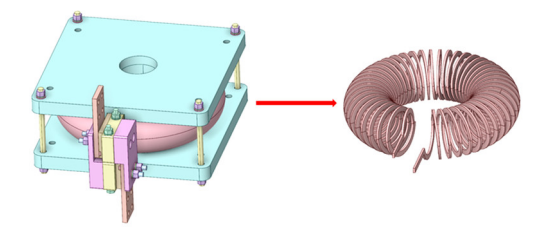
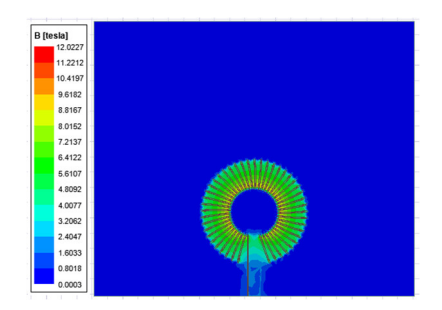
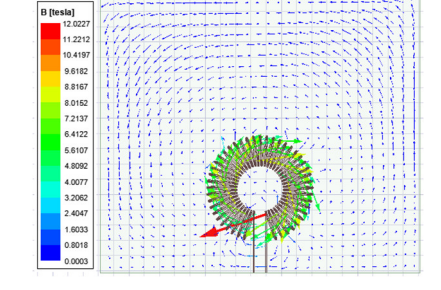


FIG 16. The structure diagram of auxiliary oscillation zero-crossing cabinet.

Fig.17. The structure diagram of helical pulse reactor pulse reactor.

A three-dimensional electromagnetic simulation model of the reactor coil was established based on ANSYS/Maxwell, and the magnetic flux density distribution is shown in FIG.18. The maximum magnetic flux density reaching 12.0227 T, meeting the operational requirements under high current pulses.



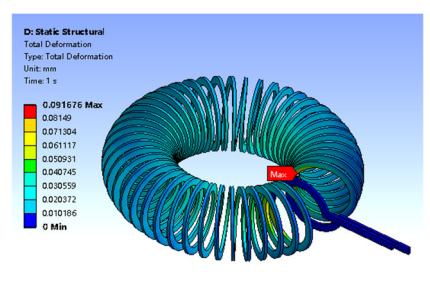


(a) Cloud map of magnetic induction intensity

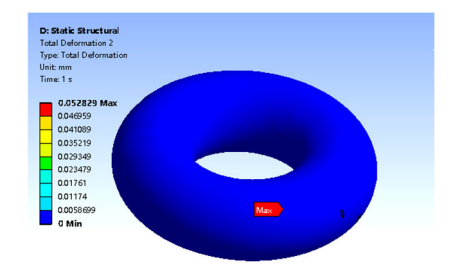
(b) Vector diagram of magnetic induction intensity

FIG.18. The magnetic flux density distribution of the pulse reactor.

A stress-strain simulation analysis of this structure was conducted using the finite element method, and the results are shown in FIG.19. The simulation indicates that the maximum deformation of the coil is 0.092 mm, and the maximum deformation of the epoxy support components is 0.053 mm, both within the material's allowable range, verifying the reliability and safety of the structural design.



(a) Coil deformation



(b) Cloud image of epoxy auxiliary parts

FIG.19. The deformation distribution of the pulse reactor.

3.4. Design and analysis of key components of PB

The structure of the PB is shown in Fig.20. The conductor parts consist of main contact, arc contact, upper copper plate, lower copper plate and cylinder current lead. Weaknesses exist in the main contact and arc contact. The PB is connected in series in the main loop of QPS.

[Left hand page running head is author's name in Times New Roman 8 point bold capitals, centred. For more than two authors, write **AUTHOR** et al.]

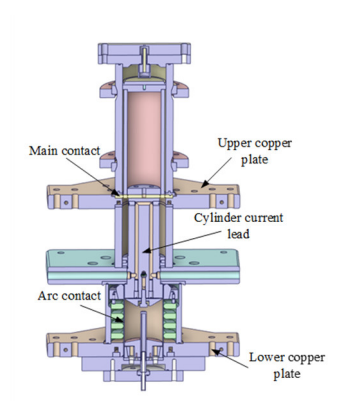


FIG.20. The structure diagram of PB.

The PB is mainly driven by RDX. During the breaking process, the arc contact is filled with deionized water. There are many weak links on the outside. The produced detonation wave cuts the arc contact laterally and expands it, producing an arc voltage of up to kV. High arc voltage can quickly transfer the loop current and quickly extinguish the arc. The shock wave generated by the main contact pushes the insulation cutting cylinder to open the main contact and strengthen the insulation.

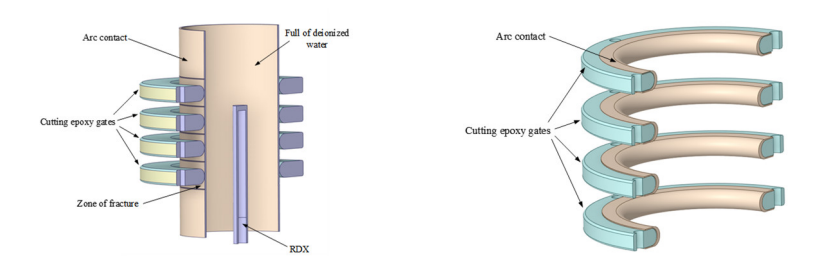


FIG.21. Schematic diagram of breaking the arc contact

Fig.22 shows the numerical model of water channel 3. The cooling water flows into the cavity from one end through a cooling water diverter and exits from the other end. Due to the high current density on the inner wall of the arc contact, the system bears a significant thermal load, making it necessary to ensure a high flow rate near the inner wall of the arc contact. Therefore, the cooling water is divided into four streams at the inlet, which are directly sprayed onto the cylinder wall to enhance the cooling effect and increase the velocity.

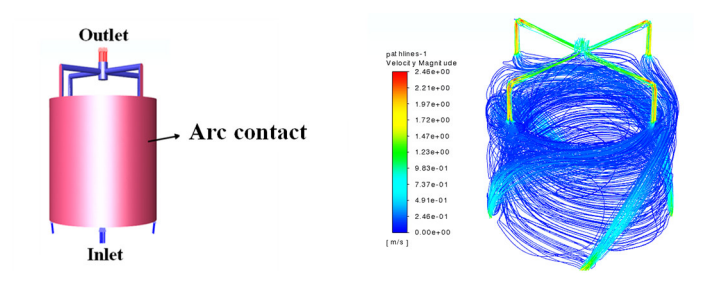


FIG.22. Schematic diagram of arc contact self-disturbing current.

4. RELIABILITY TEST OF QPS

The QPS was tested through 72 circuit breaker interruption experiments under a 70kA. In the experiments, the red waveform represents the VCB current, the purple waveform represents the total current, the blue waveform represents the resistance current, and the green waveform represents the resistance voltage.

In the FIG.23, the results show that the QPS response time is less than 240ms, and the interruption voltage meets the 4kV set requirement. All experiments completed reliable interruption under the 70kA.

[Right hand page running head is the paper number in Times New Roman 8 point bold capitals, centred]

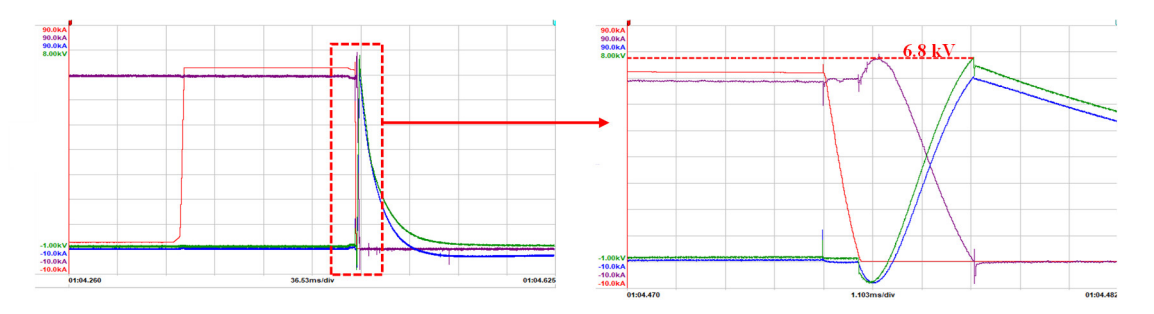


FIG.23. Interruption test waveform

5. CONCLUSION

To meet the requirements of the ITER-MCTB device, the paper presents a systematic design and optimization of the existing QPS. A permanent magnet bistable actuator has been proposed to enhance the response performance of the BPS. And an electromagnetic repulsion mechanism has been designed to improve the operating speed of the VCB. The parameters of auxiliary oscillation zero-crossing loop have been optimized, and a spiral pulse reactor has been introduced to improve commutation efficiency and stability. A self-disturbance arc contact structure has been proposed to enhance the heat dissipation and current-carrying capacity of the PB. A total of 72 reliability interruption experiments have been conducted. Under 70 kA DC conditions, the system is able to achieve a fast interruption of ≤240 ms, validating the high efficiency and stability of the designed scheme under high current conditions, fully meeting the MCTB's requirements for fast protection and safe operation.

ACKNOWLEDGEMENTS

This research was supported by the Comprehensive Research Facility for Fusion Technology Program of China. (No.2018-000052-73-01-001228).

REFERENCES

- [1] Linke, J., Du, J., Loewenhoff, T., Pintsuk, G., Spilker, B., Steudel, I., & Wirtz, M. (2019). Challenges for plasma-facing components in nuclear fusion. *Matter and Radiation at Extremes*, 4(5), 056201.
- [2] Kuzle, I., Granic, M., Holjevac, N., Capuder, T., & Pandzi', H. (2020). The future of energy. *International Journal of Electrical Power*, 123, 106318.
- [3] Mathew, M. D. (2022). Nuclear energy: A pathway towards mitigation of global warming. *Progress in Nuclear Energy*, 143, 104080.
- [4] Zylstra, A. B., et al. (2022). Burning plasma achieved in inertial fusion. *Nature*, 601, 542-548.
- [5] Zhou, Y., Li, C., Rao, B., & Yang, Y. (2025). Design and analysis of magnetic compression magnet casing based on optimized equivalent material method. *Fusion Engineering and Design*, 212, 114856.
- [6] Guan, M. Z., Wang, X. Z., Ma, L. Z., Zhou, Y., Zhao, H., Xin, C. Y., Yang, L., Wu, W., & Yang, X. (2013). Magnetic field and strain measurements of a superconducting solenoid magnet for C-ADS injector-II during excitation and quench test. *Journal of Superconductivity and Novel Magnetism*, 26, 2361-2368.
- [7] Chu, Y., et al. (2000). Design and characteristic analysis of active quench protection system for superconducting magnet. *Physica C*, *341*, 2605-2606.
- [8] Song, et al. (2011). The fast discharge system of ITER superconducting magnets. *Proceedings of the International Conference on Electrical Machines and Systems*, 1-6.
- [9] Tanchuk, V., et al. (2011). Air-cooled fast discharge resistors for ITER magnets. *Fusion Engineering and Design*, 86(6-8), 1445-1449.
- [10] Bonicelli, T., et al. (2005). The European development of a full-scale switching unit for the ITER switching and discharging networks. *Fusion Engineering and Design*, 75, 193-200.
- [11] Ge, G., Liao, M., Duan, X., Huang, Z., Huang, J., & Zou, J. (2016). Investigation on the current-zero characteristic of vacuum circuit breakers. *Vacuum*, 134, 63-68.
- [12] Zhu, J., & Li, B. (2019). Analysis and test for the DC vacuum interruption process based on the artificial current zero technology. *Electrical Machines and Control*, 23, 63-72.